Table 1 Lower limits for practicable operation of resistance wires and thermocouples (Values given are for θ_{av}, $\theta_c = 0.1$)

Sensor details	h, w cm^{-2} °C^{-1}	Static air (p)		Flux density (ρv), ($M > 2$) (g cm^{-2} sec^{-1})
		p, torr	λ/d	
Platinum wire, $2l = 2$ mm, $d = 3 \times 10^{-3}$ mm	1.9×10^{-3}	0.12	68	2.1×10^{-3}
Tungsten wire, $2l = 2$ mm, $d = 5 \times 10^{-3}$ mm	6.7×10^{-3}	0.43	24	7.4×10^{-3}
Copper/constantan thermocouple, $l_1 = l_2 = 5$ mm, $d = 25 \times 10^{-3}$ mm				
(a) Negligible bead size ($\bar{A}_1 = \bar{A}_2 = 0$)	1.0×10^{-3}	0.066	32	1.2×10^{-3}
(b) Large bead size ($\bar{A}_1 = \bar{A}_2 = 10$)	9.6×10^{-5}	0.0061	25 (bead)	1.1×10^{-4}

with solutions from equation 1 for each support wire, to the result

$$\theta_c = (T_c - T_o)/(T_f - T_o) = [(\bar{A}_1 a_1 l_1 \sinh a_1 l_1)^{-1} + (\bar{A}_2 a_2 l_2 \sinh a_2 l_2)^{-1}]/[1 + (\bar{A}_1 a_1 l_1 \tanh a_1 l_1)^{-1} + (\bar{A}_2 a_2 l_2 \tanh a_2 l_2)^{-1}] \quad (6)$$

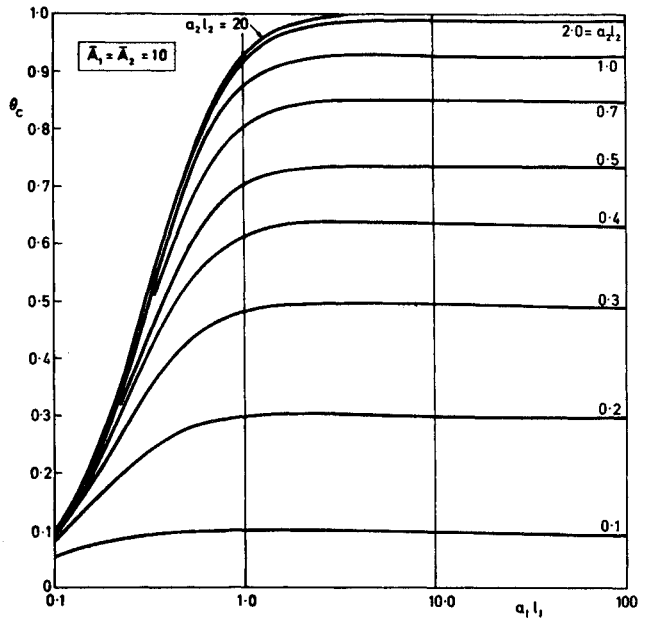

Fig. 3a Variation of thermocouple junction temperature (negligible bead size).

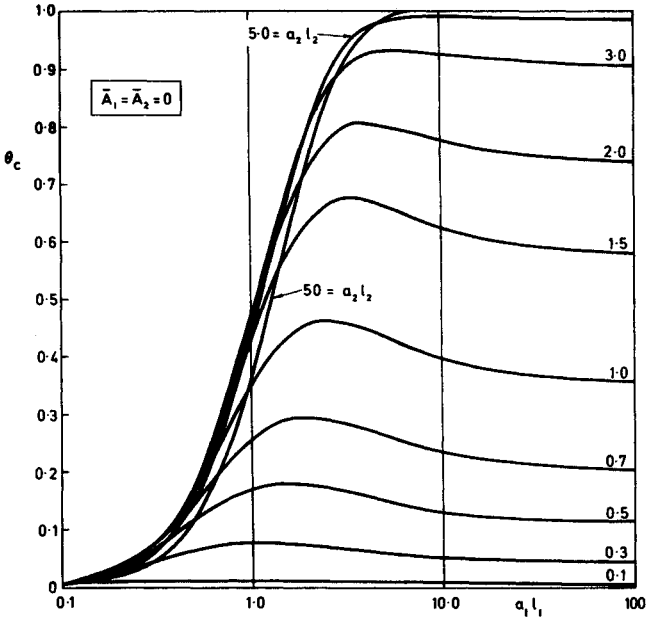

Fig. 3b Variation of thermocouple junction temperature (finite bead size, $A = 10\pi d_1 l_1 = 10\pi d_2 l_2$).

where $\bar{A}_1 = A/\pi d_1 l_1$ and $\bar{A}_2 = A/\pi d_2 l_2$. Solutions for the thermocouple response are shown in Fig. 3, assuming that the surface areas of the two support wires are equal (i.e., $\bar{A}_1 = \bar{A}_2$). It may be seen that values of both $a_1 l_1$ and $a_2 l_2$ in excess of approximately 5 are required if the thermocouple temperature is to approach the fluid temperature closely. Typical values for a copper-constantan junction supported on two 5mm wires in the gas are given in Table 1 for the cases of negligible bead size ($\bar{A}_1, \bar{A}_2 = 0$) as well as for the case of a relatively large bead ($\bar{A}_1 = \bar{A}_2 = 10$), in this case a value of $\theta_c = 0.1$ being assumed.

In conclusion, it may be seen that the solutions given provide a relatively simple means of estimating the response of resistance wire thermometers and thermocouples under conditions of marginal heat transfer between the sensor and gas. The results are of particular relevance to the measurement of gas temperatures at low pressures where significant temperature differences between gas and thermometer mountings exist.

References

[1] Rajasooria, G. P. D. and Brundrin, C. L., "Use of Hot Wires in Low-Density Flows," *AIAA Journal*, Vol. 9, No. 5, May 1971, pp. 979–981.

[2] King, L. V., "On the Convection of Heat from Small Cylinders in a Stream of Fluid," *Philosophical Transactions of the Royal Society*, A214, 1914, pp. 373–432.

[3] Kennard, E. H., *The Kinetic Theory of Gases*, McGraw-Hill, New York, 1938.

[4] Oppenheim, A. K., "Generalized theory of Convective Heat Transfer in Free Molecule Flow," *Journal of the Aerospace Sciences*, Vol. 20, 1953, pp. 49–58.

[5] Schaaf, S. A., "Heat Transfer in Rarefied Gases," *Developments in Heat Transfer*, edited by W. M. Rohsenow, M.I.T. Press, 1964, pp. 134–168.

Wind-Tunnel Wall Interference Reduction by Streamwise Porosity Distribution

CHING-FANG LO*
Arnold Air Force Station, Tullahoma, Tenn.

THE interference on the flowfield about a model caused by wind-tunnel walls is well known as one of the sources that influences the accuracy of tunnel data.[1–4] After the ventilated

Received November 11, 1971; revision received November 29, 1971. The research reported herein was sponsored by the Arnold Engineering Development Center, Air Force Systems Command, under Contract F40600-72-C-0003 with ARO Inc. Major financial support was provided by the Air Force Flight Dynamics Laboratory under Air Force Project 1366. Project monitor was Maj. P. J. Butkewicz. Further reproduction is authorized to satisfy the needs of the U.S. Government.

Index categories: Aircraft and Component Wind Tunnel Testing; Subsonic and Transonic Flow.

* Research Engineer, Propulsion Wind Tunnel Facility. Member AIAA.

wall of fixed geometry for transonic testing was invented, a variable-geometry wall was introduced to minimize the interference for different Mach numbers by varying the porosity. Calculated results[5] and experimental data[6] have shown that an optimum porosity for zero inference depends on Mach number, and an ideal wall porosity schedule as a function of Mach number can be achieved. However, this optimum porosity can only eliminate the interference at the model position. The interference still exists at the other locations along the centerline implying an interference in pitching moment as shown in Ref. 5. One set of experimental data in Ref. 1 also indicates this evidence. By using a streamwise distribution of wall porosity it is possible to eliminate pitching moment interference simultaneously with lift interference. Based on this concept, the third generation tunnel wall is being developed.

As a first step in the theoretical study, a two-dimensional perforated tunnel has been chosen for investigation. By using Fourier transform and convolution theorems, a system of integral equations is derived for a streamwise distribution of porosity. The system of integral equations has been solved by approximating the unknown functions in a series form of an independent set of functions and then calculating by the collocation method in the least squares sense.[7]

The results for a selected porosity distribution indicate that the simultaneous minimization of lift and pitching moment can be nearly achieved. The blockage interference is also calculated for the same porosity distribution. This formulation is being extended to other tunnel geometries. The promising wall configurations may be used in an experimental program at the Arnold Engineering Development Center to improve transonic wind-tunnel walls.

Analysis

For the two-dimensional inviscid subsonic flow, the linearized field equation of the perturbation velocity potential is used in the analysis. The boundary condition on the tunnel perforated wall is that the mass flow is proportional to the pressure drop across the wall expressed in the X-Y coordinates (Fig. 2) as:

$$\partial\phi/\partial X \pm [1/R(X)]\partial\phi/\partial Y = 0 \quad \text{at} \quad Y = \pm h$$

where $R(X)$ is the empirical constant or porosity parameter of a perforated wall but also a function of streamwise location.

Within the assumptions of linearized theory, the perturbation velocity potential may be decomposed into two parts, $\phi = \phi_i + \phi_m$, where ϕ_i is the interference potential caused by the presence of tunnel walls and ϕ_m is the disturbance potential induced by a model. A horseshoe vortex and a doublet are used as the mathematical model for the disturbance potential in the calculation of lift and solid blockage interferences, respectively. The linearity of the field equation and boundary conditions in the normalized coordinates $x = X/\beta h$, $y = Y/h$ gives

$$\partial^2\phi_i/\partial x^2 + \partial^2\phi_i/\partial y^2 = 0 \tag{1}$$

and

$$\frac{\partial\phi_i}{\partial x} \pm T(x)\frac{\partial\phi_i}{\partial y} = -\left(\frac{\partial\phi_m}{\partial x} \pm T(x)\frac{\partial\phi_m}{\partial y}\right), \quad y = \pm 1 \tag{2}$$

where $T(x) = \beta/R(x)$.

By using Fourier transform and convolution theorems, the transformed field equation is obtained as

$$-q^2\bar{\phi}_i + \partial^2\bar{\phi}_i/\partial y^2 = 0 \tag{3}$$

if the upstream and downstream conditions

$$\phi_i(\pm\infty) = 0 \quad \text{and} \quad \partial\phi_i/\partial x(\pm\infty) = 0$$

are satisfied. The boundary conditions are

$$-iq\bar{\phi}_i \pm (2\pi)^{-1/2}\frac{\partial}{\partial y}\left[\int_{-\infty}^{\infty}\bar{\phi}_i(\omega, y)\overline{T}(q-\omega)d\omega\right] = -\left[\overline{\frac{\partial\phi_m}{\partial x}} \pm (2\pi)^{-1/2}\int_{-\infty}^{\infty}\overline{\frac{\partial\phi_m}{\partial y}}\,\overline{T}(q-\omega)d\omega\right] \tag{4}$$

where the Fourier transformed function is defined by

$$\bar{f}(\omega) = (2\pi)^{-1/2}\int_{-\infty}^{\infty} f(x)e^{i\omega x}\,dx$$

The solution for the transformed interference potential, $\bar{\phi}_i$, is of the form

$$\bar{\phi}_i(q, y) = A(q)\sinh qy + B(q)\cosh qy \tag{5}$$

For a given disturbance potential, ϕ_m, and porosity distribution, $T(x)$, a system of integral equations for the unknown functions $A(q)$ and $B(q)$ can be obtained by substituting Eq. (5) into boundary condition Eq. (4).

Lift interference

The lift interference is calculated by using a horseshoe vortex to represent the wing model. The potential of the wing with circulation Γ at the origin of the coordinates is given as

$$\phi_m = -(\Gamma/2\pi)\tan^{-1}(y/x) \tag{6}$$

Substituting Eqs. (5) and (6) into the boundary conditions Eq. (4), one obtains the following system of integral equations,

$$A_2(q)\sinh q + (2\pi)^{-1/2}\int_{-\infty}^{\infty}A_1(\omega)\cosh\omega\overline{T}_1(q-\omega)d\omega - (2\pi)^{-1/2}\int_{-\infty}^{\infty}A_2(\omega)\cosh\omega\overline{T}_2(q-\omega)d\omega = \left(\frac{\pi}{2}\right)^{1/2}e^{-|q|} + \frac{1}{2}\int_{-\infty}^{\infty}\frac{|\omega|}{\omega}e^{-|\omega|}\overline{T}_2(q-\omega)d\omega \tag{7}$$

$$A_1(q)\sinh q - (2\pi)^{-1/2}\int_{-\infty}^{\infty}A_1(\omega)\cosh\omega\overline{T}_2(q-\omega)d\omega - (2\pi)^{-1/2}\int_{-\infty}^{\infty}A_1(\omega)\cosh\omega\overline{T}_2(q-\omega)d\omega = \frac{1}{2}\int_{-\infty}^{\infty}\frac{|\omega|}{\omega}e^{-|\omega|}\overline{T}_1(q-\omega)d\omega \tag{8}$$

where $A_1 + iA_2 = -2\pi qA/\Gamma$, $\overline{T}_1 + i\overline{T}_2 = \overline{T}$.

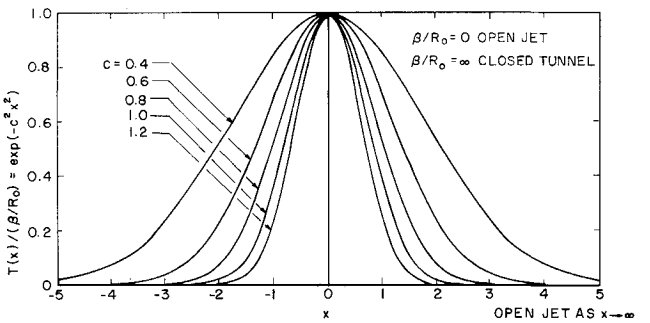

Fig. 1 Porosity distribution of the function $T(x)/(\beta/R_0) = \exp(-c^2x^2)$, where β is the compressibility factor and R_0 is the wall porosity parameter at the model location.

If the porosity distribution is chosen to be constant, the system of integral equations reduces to a system of algebraic equations. The expressions of A_1 and A_2 which are readily obtained check with those derived in Ref. 4 as expected. The specific porosity distribution is chosen as $T(x) = (\beta/R_0)\exp(-c^2x^2)$ which is plotted in Fig. 1 to depict the distribution of porosity for various values of the parameter c. This selected porosity gives the results nearly fulfilling the requirements and the mathematical simplicity. The unknown functions A_1 and A_2 are assumed in a series form as

$$A_1(q) = \sum_{n=1}^{N} a_{1n}\exp(-nq)$$
$$A_2(q) = \sum_{n=1}^{N} a_{2n}\exp(-nq) \tag{9}$$

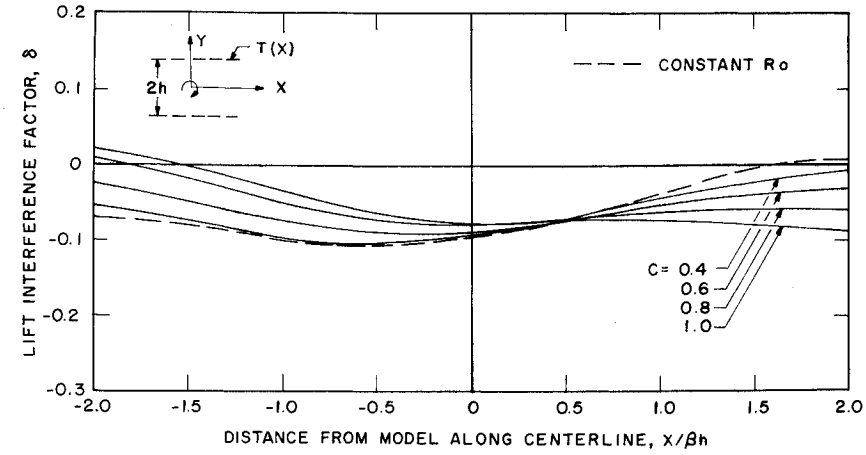

Fig. 2 Lift interference for the selected porosity $(\beta/R_0)\exp(-c^2x^2)$ with $\beta/R_0 = 1.5$.

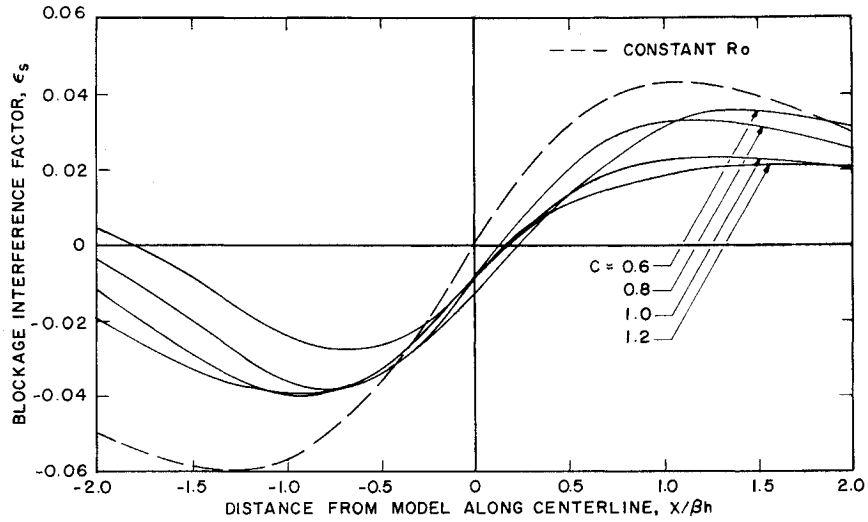

Fig. 3 Blockage interference for the selected porosity $(\beta/R_0)\exp(-c^2x^2)$ with $\beta/R_0 = 1.5$.

The reasons for choosing such series form are that the perturbation potential has satisfied the upstream and downstream conditions, that they approximate the expressions of A_1, A_2 for the uniform porosity case (Ref. 4) and that the inverse transform may be performed analytically.

After substituting the series of Eq. (9) into the integral equations, a system of algebraic equations with unknown constants a_{1n} and a_{2n} is obtained. The values of the transformed parameter q are in the range from zero to infinity. The constants a_{1n} and a_{2n} are computed by the collocation method. In choosing N values of q to yield $2n$ equations, the $2n$ unknown constants a_{1n} and a_{2n} can be determined. Improved accuracy may be achieved, however, by selecting more than N values of q to calculate a_{1n} and a_{2n} in the least squares sense. Once the constants a_{1n} and a_{2n} are determined, the interference potential in the physical plane can be obtained by the Fourier inverse formula. The lift interference factor $\delta(x)$, along the centerline may be expressed as

$$\delta(x) = \frac{h}{\Gamma}\frac{\partial \phi_i}{\partial Y} = \frac{-1}{(2)^{1/2}\pi^{3/2}} \sum_{n=1}^{N} \left[a_{1n} \frac{n}{n^2 + x^2} + a_{2n} \frac{x}{n^2 + x^2} \right]$$

The numerical calculation of a_{1n} and a_{2n} is based on 10 terms in the series Eq. (9) and 80 values of q. The lift interference at the model shown in Fig. 2 does not change significantly for the selected porosity distribution from the uniform porosity case. However, the axial gradient of the interference, hence the pitching moment interference, is greatly reduced. The curves $c = 0.8$ and 1.0 remain essentially flat in the interval $-0.5 < X/\beta h < 1.5$. Therefore, the pitching moment interference is zero for a model extending over that interval.

Blockage interference

The blockage interference is calculated similarly to the lifting interference except that a doublet is used to represent the model. The blockage interference factor, $\varepsilon_s = (\beta^3 h^2/AU)(\partial \phi_i/\partial x)$. The results in Fig. 3 indicate that the axial gradient of the blockage interference for the same selected porosity is also improved compared to that of a uniform porosity tunnel.

Conclusions

An analytic method has been developed to solve the interference problem of a tunnel with porosity distribution in the streamwise direction. The method can be applied to tunnel configurations other than the two-dimensional tunnel presented here.

A distributed porosity in the streamwise direction has been found which gives essentially zero gradient of the lift interference and also improves the blockage interference. For a two-dimensional tunnel with uniform porosity, the zero lift interference occurs at the model location only for a closed tunnel. Therefore, since it is possible to obtain essentially constant interference along the wing chord (although not zero) for the two-dimensional tunnel, it should be possible to obtain constant and zero interference for the three-dimensional tunnel.

References

[1] Ring, L. E. and Milillo, J. R., "Transonic Testing—a Review," AIAA Paper, 70-580, Tullahoma, Tenn., 1970.

[2] Ferri, A., et al., "Engine-Airplane Interference and Wall Corrections in Transonic Wind Tunnel Tests," AGARD-AR-36-71, 1971.

[3] Garner, H. C., et al., "Subsonic Wind Tunnel Wall Corrections," AGARDograph 109, 1966.

[4] Pindzola, M. and Lo, C. F., "Boundary Interference at Subsonic Speeds in Wind Tunnels with Ventilated Walls," AEDC-TR-69-47, May 1969, Arnold Engineering Development Center, Arnold Air Force Station, Tullahoma, Tenn.

[5] Lo, C. F. and Oliver, R. H., "Subsonic Lift Interference in a Wind Tunnel with Perforated Walls," *Journal of Aircraft*, Vol. 7, No. 3, May–June, 1970, pp. 281–283.

[6] Jacocks, J. L., "Evaluation of Interference Effects on a Lifting Model in the AEDC PWT 4-Ft. Transonic Tunnel," AEDC-TR-70-72, April 1970, Arnold Engineering Development Center, Arnold Air Force Station, Tullahoma, Tenn.

[7] Stokgold, I., *Boundary Values Problems of Mathematical Physics*, Vol. 1, MacMillan, New York, 1967, p. 243.

Sonic Boom of Hypersonic Vehicles

Y. S. PAN* AND W. A. SOTOMAYER†
The University of Tennessee Space Institute, Tullahoma, Tenn.

Introduction

THE phenomenon of sonic boom has received considerable attention in the past decade. Generally, the sonic boom of a supersonic aircraft can be predicted accurately, at least in the far-field, by the current sonic boom theory which is based on the well-known supersonic area rule and Whitham's supersonic projectile theory. The supersonic area rule approximates three-dimensional configurations to equivalent bodies of revolution, whereas Whitham's theory describes the far-field behavior of the flow over these bodies of revolution. The sonic boom of a hypersonic vehicle, however, cannot be predicted by the current sonic boom theory. A general "hypersonic area rule" has not yet been developed to simplify vehicle configurations, and moreover, Whitham's theory which is equivalent to a geometrical acoustic approach is not generally applicable in the hypersonic flowfield in which nonlinear effects are dominant. Indeed recent experiments have shown deficiencies of the current sonic boom theory at high Mach numbers.[1]

In this Note, we shall be concerned with the far-field flow behavior of a vehicle at hypersonic speeds. Particularly an approximate method for determining the sonic boom strength, position and the positive phase duration is presented.

Equivalence Principle

It is physically known that, at hypersonic speeds, a body leaves a long wake behind it and, at a distance sufficiently far from this body, the flowfield becomes axisymmetric. Although no studies have yet shown how a nonaxisymmetric disturbance would approach to an axisymmetric one in hypersonic flows, the flow disturbances in the far-field, to a first approximation, may be considered as those produced by an equivalent body of revolution having experienced the same total drag as the actual body. Thus we may consider a steady inviscid hypersonic flow about blunt-nosed axisymmetric slender bodies, in particular those configurations having long cylindrical after-bodies representative of the viscous wake.

It is well known in the hypersonic flow theory[2] that the steady, inviscid, hypersonic flow over slender bodies can be treated by the hypersonic-small-disturbance theory. If the streamwise coordinate x is considered as the time t, the equations in the hypersonic-small-disturbance theory are identical with the full (exact) equations for a corresponding unsteady flow in one less space variable. Consequently, the hypersonic flow over a blunted-nosed axisymmetric slender body having a long cylindrical after-body may be considered as the steady-state analogy to the constant-energy cylindrical blast wave problem.[3] The nose drag in the steady problem is equivalent to the finite energy which is instantaneously released in the unsteady problem.

In the far-field of a slender body, the flow is only slightly disturbed and shock waves are already weak even in the hypersonic flow. The governing equations for the steady hypersonic flow in the far-field can be linearized. The linearized equations for the steady hypersonic flow with the streamwise coordinate x replaced by $Ut(1-M^{-2}) \approx Ut$ are exactly analogous to the unsteady two-dimensional acoustic equations.[4] (U and M are the freestream velocity and Mach number, respectively.) Therefore, the equivalence of the steady three-dimensional flow with the unsteady two-dimensional flow exists in the entire hypersonic flowfield over slender bodies.

Unsteady Cylindrical Wave

Solutions to the unsteady two-dimensional problem with cylindrical symmetry have been found only in the limiting cases of very strong[3] and very weak shock wave.[5] Attempts to extend these solutions to the intermediate strength of shock waves by using series expansion have not been very successful. Recently, Plooster[6] has obtained several numerical solutions for cylindrical shock waves from line sources. His computations extend blast wave solutions well into the weak shock region. For the purpose of determining sonic booms, Plooster's lowest data of shock strength 0.1 are still too high to be directly applicable. (For example, the sonic booms for SST are about the order of 10^{-3}.) Hence, we shall extrapolate Plooster's numerical data for the case of line source idea gas to the weak shock region.

The propagation of weak shock waves can be described by the weak shock theory based on the geometrical acoustics.[5] By calculating the rays and ray-tube areas, the pressure disturbance at any point can be determined from a given initial disturbance. Now we assume that the weak shock theory may be matching directly with Plooster's data for the lowest shock overpressure $[(\Delta p/p_o)_s \simeq 0.1]$ signature. This assumption can be justified quantitatively and qualitatively.[4] Following the procedure described above or used in the current sonic boom calculation, complete pressure signatures can be obtained at any distance farther afield.

Since the positive phase overpressure signature of Plooster $[(\Delta p/p_o)_s \simeq 0.1]$ is linearly varied with the space coordinate, this linear variation will remain in the farther afield. The positive overpressure signature, which is important in the calculation of the sonic boom impact, can be specified by the shock overpressure $(\Delta p/p_o)_s$, shock location t_s vs r_s and the duration of the positive phase L. By matching Plooster's data, $[(\Delta p/p_o)_s = 0.1]$, with the weak shock theory

$$(\Delta p/p_o)_s = 0.343/\lambda_s^{1/2}(\lambda_s^{1/2} - 0.908)^{1/2} \quad (1)$$

$$\tau_s = \lambda_s - 0.160 - 0.588(\lambda_s^{1/2} - 0.908)^{1/2} \quad (2)$$

$$l = 0.588(\lambda_s^{1/2} - 0.908)^{1/2} \quad (3)$$

Here $\tau = C_o t/R_o$, $\lambda = r/R_o$ and $l = L/R_o$, with C_o being the sound speed of the undisturbed flow, R_o a characteristic radius $(E/b\gamma p_o)^{1/2}$, E the energy released per unit length of the line source and $b = 0.985$ for air with $\gamma = 1.4$[7].

The accuracy of the above extrapolation formula, Eqs. (1–3) can be examined. By matching the weak shock theory with Plooster's signature of shock overpressure 0.19, which is 90% higher than that for Eqs. (1–3), we found that the new results differ from Eqs. (1–3) by less than one percent. This justifies our assumption that the weak shock theory can be directly matched with Plooster's lowest shock overpressure signature $[(\Delta p/p_o)_s = 0.1]$.

Sonic Boom Signatures

After having obtained a solution for the unsteady cylindrical wave, we may find the flow pattern of a hypersonic blunt-nosed axisymmetric slender body by proper changes of the variables. By the use of the blast wave analogy, the energy released per unit length of line source is replaced by the total drag of the body and, in turn, can be related to the drag coefficient C_D, dimension d and freestream conditions ρ_o, U of the body,

$$E = D = (\pi/8)(C_D d^2 \rho_o U^2) \quad (4)$$

By using the equivalence principle, the nondimensional variables τ and λ may be expressed in the space variables x and r, respectively, with the parameters M, C_D and d,

Received November 3, 1971.

* Associate Professor of Aerospace Engineering. Member AIAA.

† Graduate Student, Air Force Institute of Technology; presently ASD/ENCES, Wright-Patterson Air Force Base, Ohio.